10-9-2018

Reverse-engineering of graphene on metal surfaces: a case study of embedded ruthenium

Ann Lii-Rosales
Iowa State University and Ames Laboratory, ylii@iastate.edu

Yong Han
Ames Laboratory, y27h@iastate.edu

Ka Man Yu
The Hong Kong University of Science and Technology

Dapeng Jing
Iowa State University and Ames Laboratory, djing@iastate.edu

Nathaniel Anderson
Iowa State University and Ames Laboratory, naa@iastate.edu

See next page for additional authors

Reverse-engineering of graphene on metal surfaces: a case study of embedded ruthenium

Abstract
Using scanning tunneling microscopy, x-ray photoelectron spectroscopy, and x-ray absorption spectroscopy, we show that Ru forms metallic nanoislands on graphite, covered by a graphene monolayer. These islands are air-stable, contain 2–4 layers of Ru, and have diameters on the order of 10 nm. To produce these nanoislands two conditions must be met during synthesis. The graphite surface must be ion-bombarded, and subsequently held at an elevated temperature (1000–1180 K) during Ru deposition. A coincidence lattice forms between the graphene overlayer and the Ru island top. Its characteristics—coincidence lattice constant, corrugation amplitude, and variation of carbon lattice appearance within the unit cell—closely resemble the well-established characteristics of single-layer graphene on the (0001) surface of bulk Ru. Quantitative analysis of the graphene lattice in relation to the coincidence lattice on the island tops show that the two-dimensional lattice constant of the underlying metal equals that of bulk Ru(0001), within experimental error. The embedded Ru islands are energetically favored over on-top (adsorbed) islands, based on density-functional-theory calculations for Ru films with 1–3 Ru layers. We propose a formation mechanism in which Ru atoms intercalate via defects that act as entry portals to the carbon galleries, followed by nucleation and growth in the galleries. In this model, high deposition temperature is necessary to prevent blockage of entry portals.

Keywords
graphite, ruthenium, intercalation, surface, STM, DFT, moiré superlattice

Comments
This is a peer-reviewed, un-copyedited version of an article accepted for publication/published in *Nanotechnology*. IOP Publishing Ltd. is not responsible for any errors or omissions in this version of the manuscript or any version derived from it. The Version of Record is available online at DOI: 10.1088/1361-6528/aae1e3.

Authors
Ann Lii-Rosales, Yong Han, Ka Man Yu, Dapeng Jing, Nathaniel Anderson, David Vaknin, Michael C. Tringides, James W. Evans, Michael S. Altman, and Patricia A. Thiel

Reverse-Engineering of Graphene on Metal Surfaces: A Case Study of Embedded Ruthenium

Ann Lii-Rosales,[1,2] Yong Han,[1] Ka Man Yu,[3] Dapeng Jing,[1,4] Nathaniel Anderson,[1,5] David Vaknin,[1,5] Michael C. Tringides,[1,5] James W. Evans,[1,5] Michael S. Altman,[3] and Patricia A. Thiel[1,2,6]

[1] Ames Laboratory, Ames, IA 50011 USA
[2] Department of Chemistry, Iowa State University, Ames, IA 50011 USA
[3] Department of Physics, The Hong Kong University of Science and Technology, Hong Kong, China SAR
[4] Materials Analysis and Research Laboratory, Iowa State University, Ames, IA 50011 USA
[5] Department of Physics and Astronomy, Iowa State University, Ames, IA 50011 USA
[6] Department of Materials Science and Engineering, Iowa State University, Ames, IA 50011 USA

Key words: Graphite, ruthenium, intercalation, surface, STM, DFT, moiré superlattice, coincidence lattice

Abstract.

Using scanning tunneling microscopy, X-ray photoelectron spectroscopy, and X-ray absorption spectroscopy, we show that Ru forms metallic nanoislands on graphite, covered by a graphene monolayer. These islands are air-stable, contain 2-4 layers of Ru, and have diameters on the order of 10 nm. To produce these nanoislands two conditions must be met during synthesis. The graphite surface must be ion-bombarded, and subsequently held at elevated temperature (1000-1180 K) during Ru deposition. A coincidence lattice forms between the graphene overlayer and the Ru island top. Its characteristics – coincidence lattice constant, corrugation amplitude, and variation of carbon lattice appearance within the unit cell – closely resemble the well-established characteristics of single-layer graphene on the (0001) surface of bulk Ru. Quantitative analysis of the graphene lattice in relation to the coincidence lattice on the island tops shows that the two-dimensional lattice constant of the underlying metal equals that of bulk Ru(0001), within experimental error. The embedded Ru islands are energetically favored over on-top (adsorbed) islands, based on density-functional-theory calculations for Ru films with 1-3 Ru layers. We propose a formation mechanism in which Ru atoms intercalate via defects that act as entry portals to the carbon galleries, followed by nucleation and growth in the galleries. In this model, high deposition temperature is necessary to prevent blockage of entry portals.

1. Introduction.

Growth of graphene on metal substrates has been studied extensively.[1-3] It generally involves decomposition of a hydrocarbon precursor on the metal substrate at elevated temperatures, or high temperature segregation of carbon to the metal surface from the bulk.[1] Both scenarios start with a bulk metal substrate, followed by addition of a carbon source to grow the graphene overlayer. However, one could envision reverse-engineering the synthesis of supported graphene, by using multilayer graphene (i.e., graphite) as the starting point, and inserting the metal beneath the surface graphene layer. This reverse-engineering of supported graphene would be in some ways similar to the formation of bulk graphite intercalation compounds (GICs),[4] wherein non-graphitic atoms or molecules are inserted into galleries between graphene sheets. Several families of elemental metals are known to form GICs, including alkali metals, alkaline earths, and rare earths. However, elemental transition and noble metals (on which graphene is typically grown) do *not* form GICs.[4]

Recently, we have demonstrated that multilayer islands of the rare earth Dy and the transition metal Cu can be grown beneath the surface of graphite, and furthermore provided comprehensive analysis of the conditions under which this outcome is achieved.[5-6] These results are unanticipated and novel on two fronts: First, a metal that is *not* known to form a GIC (Cu) can be embedded at the graphite surface. Second, the form of the embedded metal, for both Dy and Cu, is much different than known GICs. For instance, Dy atoms in GICs arrange in a dilute $(\sqrt{3}\times\sqrt{3})R30°$ structure in a single Dy atomic layer,[7] which is quite distinct from a metallic multilayer. For both Dy and Cu, the synthesis of encapsulated islands requires: (1) Defects created in the graphite surface *before* metal deposition, presumably to provide entry into the carbon galleries;[8] and (2) Metal deposition *at* elevated substrate temperature. The optimal deposition temperature is about 800 K for Cu and 850 K for Dy. Previously, we reported a preliminary observation that Ru also could form encapsulated multilayer islands, but no comprehensive analysis of the preparation conditions or resultant islands. In this paper, we will explore the synthetic conditions necessary for islands of Ru metal to grow beneath the graphite surface, we will characterize the islands extensively, and we will examine the energetics involved.

Among metal substrates for graphene, Ru has received considerable attention, partly because graphene can grow into well-ordered and contiguous layers over large areas on Ru(0001), without the large-angle rotational domains characteristic of many other metals.[9] Monolayer and bilayer graphene on Ru(0001) have been well studied and characterized via microscopy and diffraction techniques.[1-2, 9-12] The results from these earlier studies serve as useful benchmarks for comparison with the present work. In particular, earlier work has revealed that a coincidence lattice, also commonly called moiré superlattice, forms due to lattice mismatch between a graphene monolayer (GML) and the (0001) surface of bulk Ru.[9-10, 13-15] We refer to this combined system as GML/Ru(0001). Similar moirés have been reported for GMLs on other metals.[1-3] The positions of coincidence occur periodically when different integer numbers of fundamental unit cells in the carbon and metal layers span the same real-space distance in a common direction. The moiré formed by GML/Ru(0001) has average periodicity 2.93 ± 0.08 nm.[10] This corresponds to 10.8 ± 0.3 times the nearest-neighbor distance on bulk Ru(0001), which is 0.271 nm.[16] A diffraction study has suggested that the apparent moiré is actually a higher-order coincidence lattice, with (2×2) features in the large coincidence unit cell.[17] In STM, the moiré unit cell is characterized by a periodic corrugation with typical vertical

magnitude of 0.1 nm.[9-10, 18-20] The competing influences of electronic effects and structural effects in producing this corrugation in STM images has been discussed.[21-22]

Ru finds wide applications in catalysis. Not only is Ru used in organic syntheses, it is also the most active Fischer-Tropsh catalyst.[23] The catalytic properties of Ru can be improved by coupling Ru with a carbonaceous support, such as graphene, carbon nanotubes, and graphite nanofibers.[24-27] The advantages associated with carbonaceous supports suggest that surface encapsulation of Ru in graphite may offer new and exciting surface properties with promise in heterogeneous catalysis. The embedded metal may be physically and chemically accessible by virtue of being near the surface. Furthermore, surface encapsulation may offer scaffolding and fixation to prevent particle coarsening, noting that coarsening is a ubiquitous pathway leading to catalysis degradation.[27]

This paper is organized as follows. Both experimental and theoretical methods are described briefly in Sec. 2. Then, results are presented in Sec. 3, followed by a discussion in Sec. 4. Section 5 presents conclusions. Supplemental Information (SI) is also provided, with content indicated throughout the text.

2. Experimental and Computational Methods.

Experimental methods. Experiments were performed in an Omicron ultrahigh vacuum (UHV) chamber with base pressure of 2×10^{-11} mbar. In short, Ru was deposited via physical vapor deposition from an *e*-beam evaporator onto commercially available highly-oriented pyrolytic graphite (HOPG, ZYA grade). The Ru flux was 0.1 monolayer/minute. The graphite surface was either pristine (cleaved using Scotch tape) or defect-rich (bombarded with argon ions). Ru was deposited onto either type of surface while the graphite sample was held at different temperatures T_{dep}. T_{dep} ranged from 300 K to 1180 K, 1180 K being the maximum accessible with our apparatus. Major characterization techniques included scanning tunneling microscopy (STM; images were acquired in constant-current mode) and X-ray photoelectron spectroscopy (XPS), both performed in UHV with the sample at room temperature. In addition, some X-ray absorption spectroscopy (XAS) experiments were performed in high vacuum (pressure in the 10^{-9} mbar range) on samples that had been transported *ex situ* in air. Further details are available in the SI.

Computational methods. First-principles density-functional-theory (DFT) total-energy calculations were performed for the Ru system using the plane-wave VASP code.[28] The projector-augmented-wave (PAW) method[29] was used for the electron-core interactions, and the optB88-vdW functional, where the exchange functional was optimized for the correlation part,[30] was used to approximately account for dispersion interactions. The pseudopotentials were generated and released in 2013 by the VASP group. Spin-polarization effects and dipole corrections were taken into account in all DFT calculations. The Γ-centered $\boldsymbol{k}$ mesh was system-specific and will be given individually. A series of benchmark calculations was carried out for the graphite lattice and the pure metal, as described in the SI.

3. Results.

3.1. Characterization of Graphite Surfaces.

Detailed characterization and descriptions of pristine (*p*-) and ion-bombarded (*i*-) graphite surfaces are available elsewhere.[5-6] In short, *p*-graphite has flat and smooth terraces. Triangular arrays of C atoms (3 out of 6 atoms in each hexagon) can be resolved, with lattice spacing of 0.247 ± 0.003 nm. This agrees well with the literature value of graphite lattice spacing, 0.246 nm.[31] After subjecting *p*-graphite to ion bombardment, surface defects appear as bright protrusions with height ≤ 0.35 nm. STM reveals that these defects adopt a variety of shapes and sizes. Some are similar to single-atom vacancies with three-fold symmetry.[8, 32-33] Other types presumably include multi-atom vacancies and interstitial C.[33-35] Evidence of electronic perturbation is often present around defects, manifested as a well-known $(\sqrt{3}\times\sqrt{3})R30^{o}$ superlattice.[36-37]

3.2. Effect of T_{dep} on Ru Growth.

Figure 1 shows representative STM images after five separate depositions of Ru on *i*-graphite at various temperatures. At T_{dep} = 300 K (Fig. 1a,b), the Ru coverage is 2.4 ± 0.18 monolayers and the Ru simply forms round clusters (1.04 ± 0.13 nm tall) that are stable under tunneling conditions. At a much higher T_{dep} of 900 K (Fig. 1d,e), the Ru clusters are taller and wider than at 300 K. The appearance of Ru clusters deposited on *i*-graphite in this temperature range is very similar, qualitatively, to that reported in an earlier study by Nielsen et al., although it is notable that they did not explore deposition temperatures above 950 K for *i*-graphite.[38] In our work, starting at 1000 K (Fig. 1g,h), fewer clusters decorate the surface compared to 900 K. In addition to the tall (bright) clusters with round tops, short (dim) islands with flat tops emerge (examples are marked by arrows in Fig. 1h). At slightly higher temperature, 1050 K (Fig. 1j,k), the short islands are more apparent. At 1180 K (Fig. 1m,n) they predominate, and have an average diameter of 13 nm. More STM images following deposition at 1180 K are shown in the SI. Based upon evidence to follow, we assign the tall features as bare Ru clusters, and short features as Ru islands covered by a graphitic overlayer.

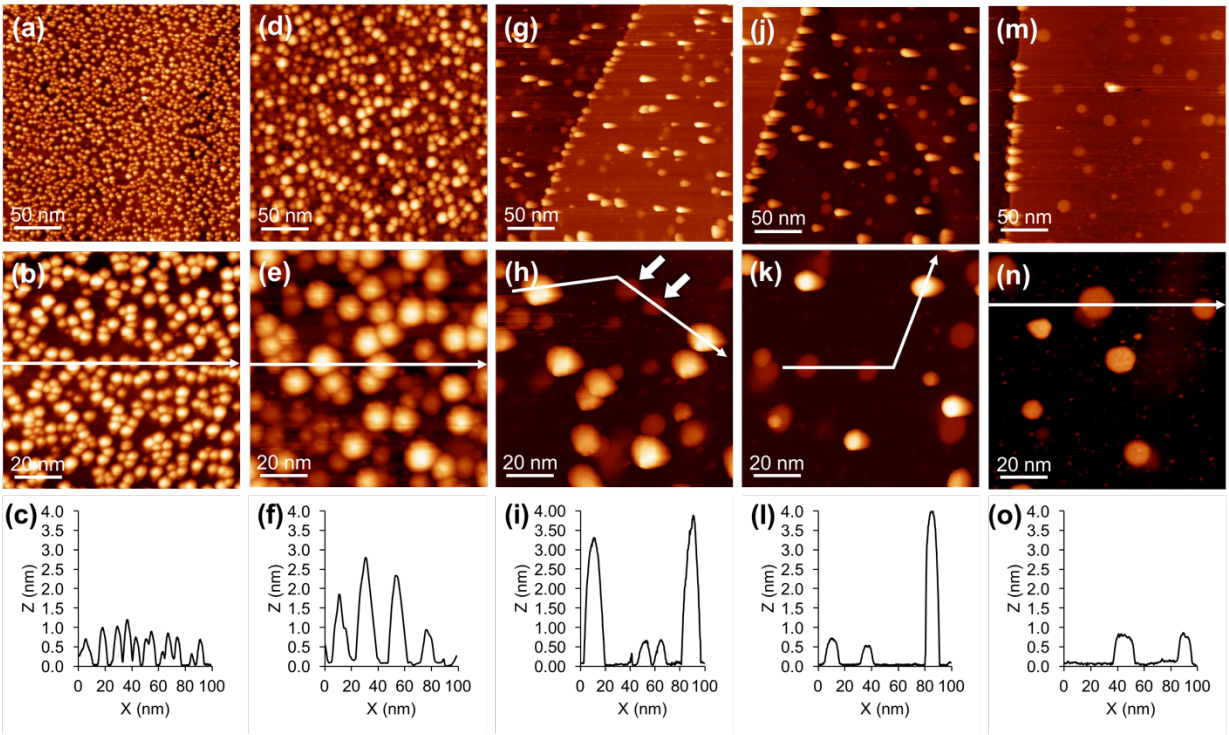

Figure 1. Representative topographic STM images, and corresponding line profiles, after five separate depositions of Ru on *i*-graphite at (a-c) 300 K, (d-f) 900 K, (g-i) 1000 K, (j-l) 1050 K, and (m-o) 1180 K. In (h), two examples of short features are marked by arrows. In (n), all islands are short, illustrating the progression from predominantly tall to short features. Tunneling conditions are: (a,b) +4.8 V, 0.27 nA; (d,e) +4.5 V, 0.25 nA; (g) +1.0 V, 0.26 nA; (h) +1.2 V, 0.27 nA; (j,k) +1.1 V, 0.26 nA; (m) +1.2 V, 0.27 nA; and (n) +1.6 V, 0.27 nA.

Several control experiments are performed to further determine conditions favorable to the short islands. First, Ru is deposited on *i*-graphite at 300 K (Fig. 2a,b; 2g,h) and then heated. In one experiment, the final temperature is 1070 K (Fig. 2d,e). In a second experiment, the final temperature is 1180 K (Fig. 2j,k). In both cases, clusters coarsen, based on increased cluster sizes and decreased density, but the short islands do not appear. These experiments demonstrate that deposition *at* elevated temperature is necessary to produce the short islands. In a third experiment, Ru is deposited on *p*-graphite at 1000 K (Fig. 2m,n). Only tall clusters are observed, without the short islands seen on *i*-graphite at 1000 K. This shows that defects introduced by ion bombardment are essential to produce the short islands.

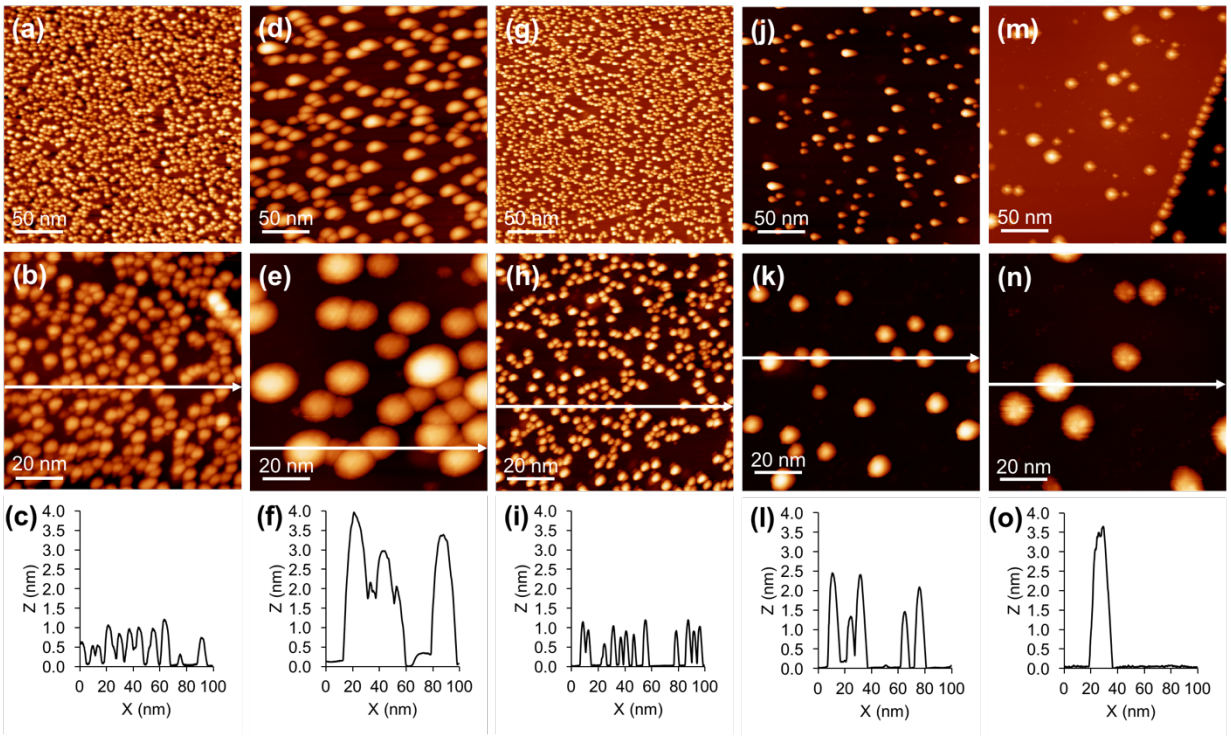

Figure 2. Control experiments. Topographic STM images of ~3.1 ML of Ru deposited on (a,b) *i*-graphite at 300 K followed by (d,e) annealing at 1070 K for 20 minutes. A separate experiment of ~2.5 ML of Ru deposited on (g,h) *i*-graphite at 300 K followed by (j,k) annealing at 1180 K for 20 minutes. (m,n) Topographic STM images of Ru deposited on *p*-graphite at 1000 K. Corresponding line profiles are shown in (c,f,i,l,o). Tunneling conditions are: (a,b) +4.8 V, 0.27 nA; (d) +1.8 V, 0.27 nA; (e) +3.0 V, 0.27 nA; (g) +2.0 V, 0.26 nA; (h) +1.8 V, 0.26 nA; (j,k) +2.8 V, 0.26 nA; (m) +1.7 V, 0.26 nA; and (n) +1.1 V, 0.26 nA.

At temperatures where tall clusters and short islands coexist, 1000 K < T_{dep} < 1180 K, the tall clusters are 2 – 4 nm tall, while short islands are at most 1.3 nm tall (Fig. 3a). There is no overlap in their height distributions. On average, the heights of tall clusters decrease slightly, and heights of short features increase, as T_{dep} increases. In addition, error bars in Fig. 3a reflect the fact that tall clusters exhibit a much larger range of heights than short islands.

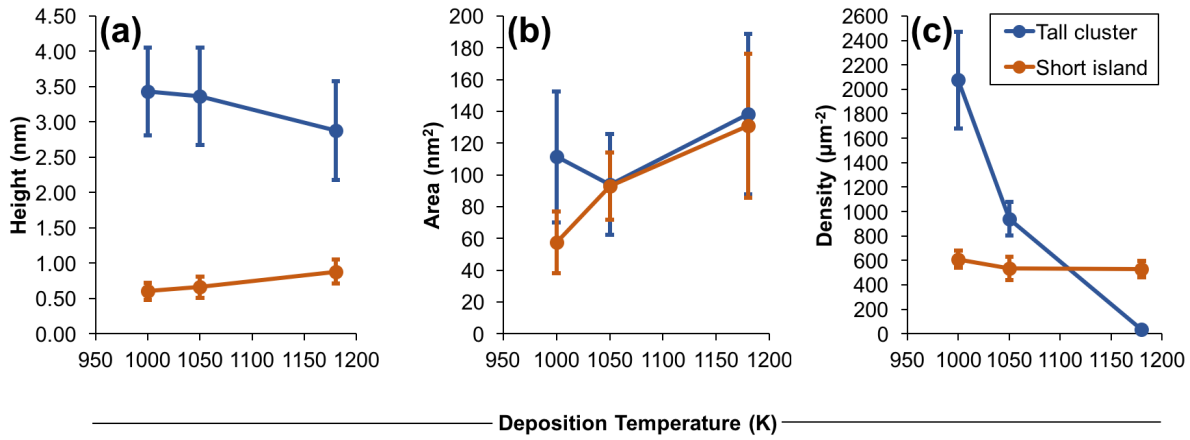

Figure 3. Average characteristics of Ru clusters and islands as functions of deposition temperatures. Values for individual data points are given in Table 1 in the SI. All measurements are from features on terraces only.

The area and density of islands are shown in Fig. 3b-c, respectively. Together with heights, these allow the volume fractions and volume changes to be estimated. Assuming pillar-like shapes, the volume encompassed by tall features represents about 90% of the total volume at 1000 K, and decreases by a factor of 150 at 1180 K, while the total volume of the short features increases only by a factor of 6. Thus there is a strong net decrease in Ru coverage, which is likely due to increasing desorption/reflection of the metal during deposition in this temperature range. It is remarkable that the short islands grow, both in size and density, in this regime.

We use XPS to compare the binding energy (B.E.) values of Ru peaks at different deposition temperatures to determine the chemical state of the deposited metal. Figure 4a-c represents three experiments where Ru is deposited on *i*-graphite at 300 K, 1000 K, and 1180 K. The most prominent XPS peaks of Ru are the $3d_{5/2}$ and $3d_{3/2}$, but because they overlap with the strong C 1*s* peak, deconvolution is necessary.[39] The established B.E. of metallic Ru $3d_{5/2}$ is 279.75 ± 0.37 eV according to a survey of existing literature values.[39] Our measured B.E. (after deconvolution) falls in this range, at 279.85-280.06 eV; exact values are given in Fig. 4 caption. On average, there is a slight downward shift of 0.14 eV from 300 K to 1180 K. Even though this is statistically significant, it is questionable in light of the uncertainty due to deconvolution from the large C peak. At the same time, there is no significant change in the deconvoluted C 1*s* peak position or shape, nor in its shake-up satellite at 291 eV or plasmon-loss satellites at 293.1 eV and 288.7 eV. We conclude that XPS is effectively insensitive to the transition from bare Ru clusters to embedded Ru islands in these experiments, indicating that Ru is in a bulk-like metallic state in both configurations.

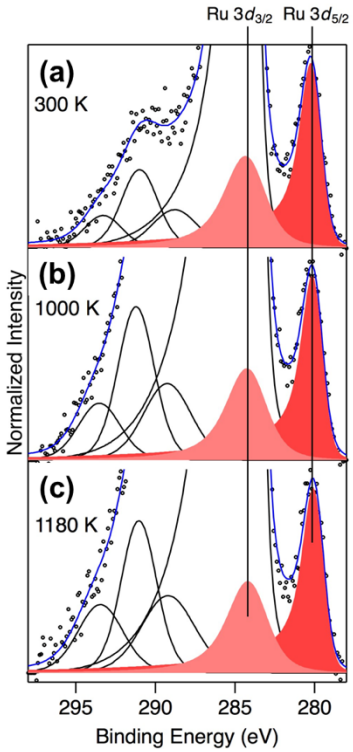

Figure 4. (a-c) XP spectra of Ru deposited on *i*-graphite at various deposition temperatures. The vertical lines show the average binding energy of Ru $3d_{3/2}$ and Ru $3d_{5/2}$ peaks at 284.1 and 280.0 eV. Solid black curves show the C 1*s* main peak (truncated) and its loss features. Solid blue line shows the overall fit to the experimental data points. Intensities are normalized to the Ru $3d_{5/2}$ peak. The average B.E. of the deconvoluted $3d_{5/2}$ peak is: 280.03 ± 0.02 eV at 300 K; 279.96 ± 0.02 eV at 1000 K; and 279.89 ± 0.03 eV at 1180 K. Each value is an average over four separate XPS acquisitions.

3.3. Characterization of Embedded Ru Islands.

Presence of graphitic overlayer. High-resolution STM images reveal a graphitic layer atop the short islands. Figure 5 shows examples. Carbon atoms are resolved throughout each image, appearing as hexagonally-arranged bumps with spacing of 0.247 ± 0.002 nm on the graphite substrate, and 0.247 ± 0.003 nm atop the islands. Furthermore, the carbon lattice extends continuously over the edges of the islands, as demonstrated by the three-dimensional views in Fig. 5d-f. This provides firm evidence that the short islands are embedded. Defects are present on top of some Ru islands, but they are less common than defects on the surrounding *i*-graphite.

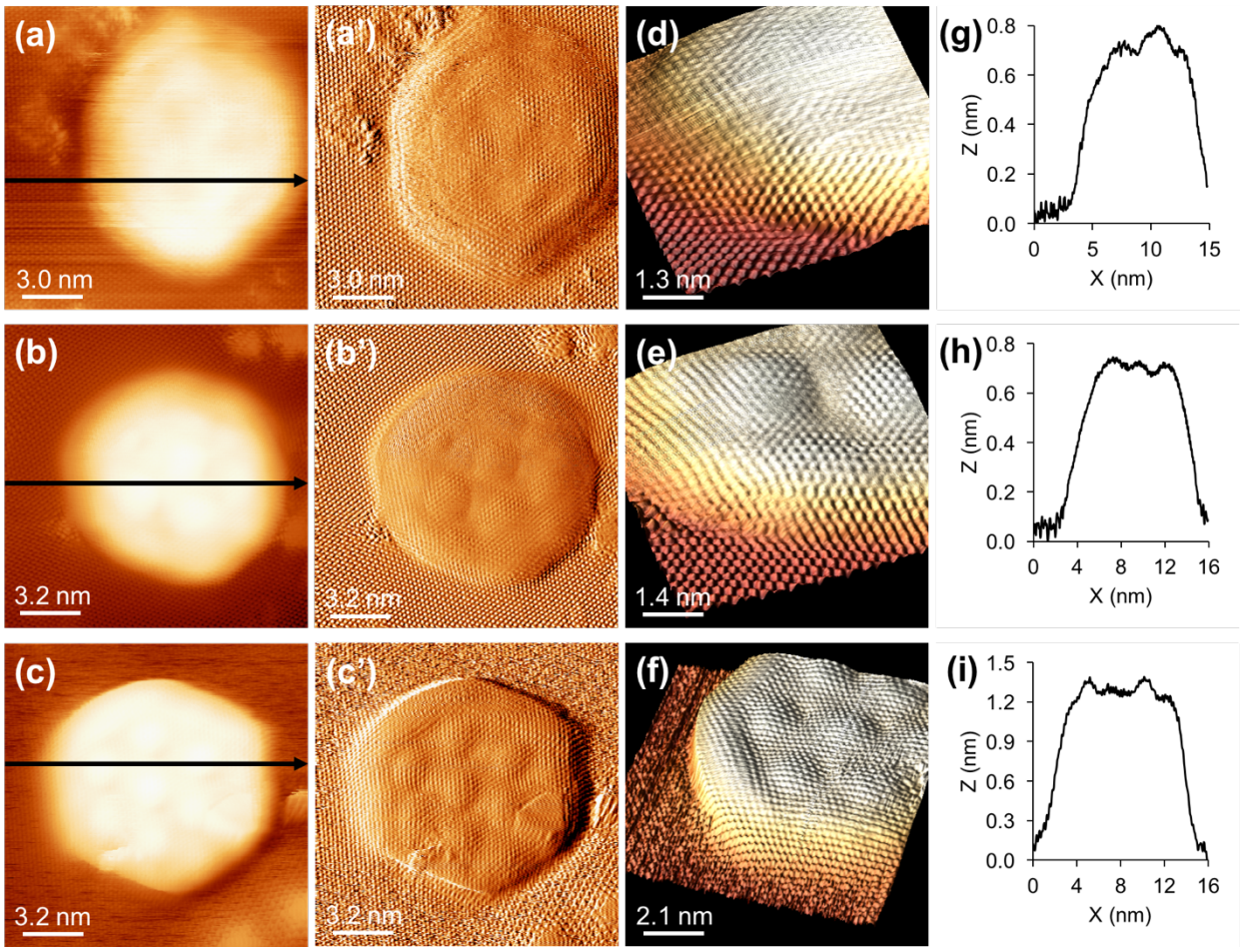

Figure 5. Representative high-resolution STM images of embedded Ru islands (the "short" islands in Figure 1). An island from each T_{dep} is shown in (a) 1000 K, (b) 1050 K, and (c) 1180 K. (a',b',c') are corresponding derivative images. Panels (d-f) show three-dimensional images of different islands grown at (d,e) 1050 K and (f) 1180 K. Corresponding line profiles are shown in (g-i). Tunneling conditions are: (a) +55 mV, 0.41 nA; (b) +4 mV, 0.41 nA; (c) +20 mV, 0.50 nA; (d) +3 mV, 0.41 nA; (e) +4 mV, 0.41 nA; and (f) +20 mV, 0.50 nA.

By contrast, the high-resolution image in Fig. 6a shows a tall cluster at the edge of a short island. Such a configuration is uncommon. The contrast in height of these two features is demonstrated in the line profile in Fig. 6b. As shown in Fig. 6c-d, the carbon lattice on both the graphite substrate and the embedded island is atomically resolved. However, the carbon lattice is absent on top of the tall cluster, which shows irregular features instead. This direct comparison supports the assignment of the tall clusters as bare Ru.

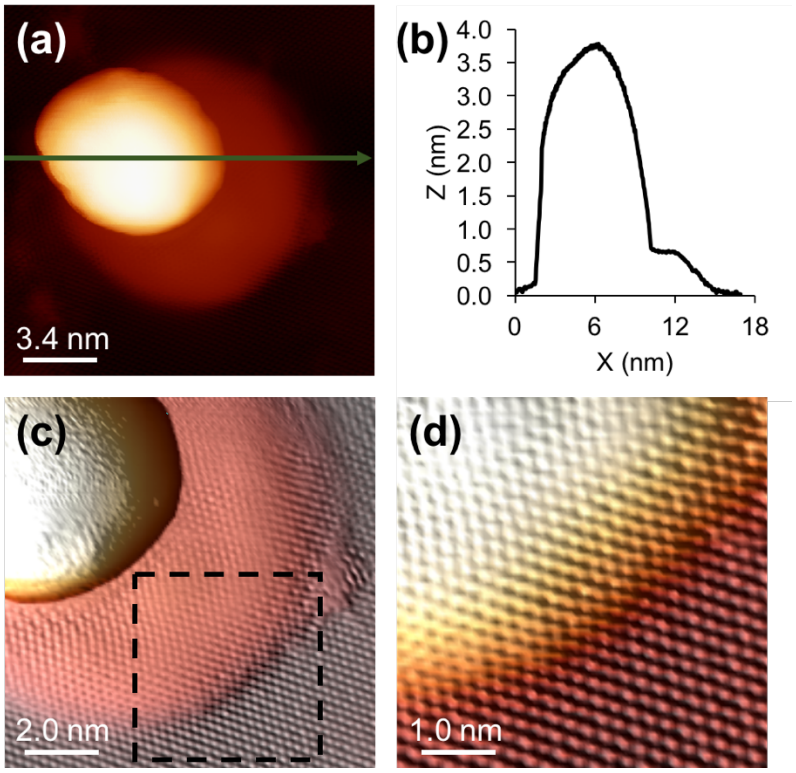

Figure 6. (a) STM image of a tall cluster supported on an embedded island. Line profile in (b) shows the contrasting heights. (c) A semi-three-dimensional image to highlight the C lattice that is resolved on both the graphite substrate and embedded island, but not on the tall cluster because it is bare (not embedded). (d) is enlarged from the boxed area in (c), showing the continuity of the C lattice over the edge of the embedded island. Tunneling conditions are: (a,c,d) +7 mV, 0.42 nA.

Shapes. The embedded islands often have hexagonally-faceted footprints, suggestive of metallic Ru, in accord with the XPS data (Sec. 3.2). Examples are visible in Fig. 1n, and Fig. 5a-c. The six-fold symmetry is consistent with hcp packing.[40] Rarely, a triangular shape is observed, indicating fcc stacking.[40]

Moiré characteristics. Also evident in the STM images are regular features at longer length scale – the larger protrusions in Fig. 5. These indicate a coincidence lattice that forms due to lattice mismatch between the graphite layer and the metal. As described in Sec. 1, such coincidence lattices, also called moiré superlattices, are well known for the related system GML/Ru(0001).[2-3, 9-10] The moiré periodicity for embedded Ru islands, averaged over all three temperatures, is 2.97 ± 0.13 nm. This compares well with the value reported for GML/Ru(0001), 2.93 ± 0.08 nm.[10] The magnitude of the corrugation measured by STM in this work falls in the range 0.07-0.15 nm, also comparable to the range of STM measurements for GML/Ru(0001), 0.08-0.15 nm.[9-10, 18-20] It is known that the corrugation can be bias-dependent; however, the range of tip voltages used in this work is V_t = +1.0 to +1.8 V, where there is little or no bias dependence.[19] The existence of the moiré and its dimensions thus support the identification of the short features as well-ordered, bulk-like Ru islands with their close-packed (0001) faces parallel to the graphite surface.

Quantitative moiré analysis. Information about the structure of embedded Ru islands can be obtained by quantitative analysis of the experimentally-measured quantities that characterize the moiré superlattice and graphite layer, i.e., moiré periodicity or coincidence lattice constant (a_c), graphite lattice spacing (a_g), and relative orientation (θ_c) of the coincidence lattice with respect to the graphite lattice. This analysis yields, in particular, the Ru lattice constant, a_{Ru}, and the relative orientation of the Ru lattice, θ_{Ru}, with respect to the graphite lattice. The approach and detailed results for all islands studied are described in the SI.

The average Ru lattice constant determined for a set of 18 islands is $a_{Ru} = 0.269 \pm 0.003$ nm and the average orientation is $\theta_{Ru} = 0.211° \pm 0.128°$. This value of a_{Ru} equals the bulk value, 0.271 nm, within statistical uncertainty. Note that evidence of the slight misalignment of the GML grown on bulk Ru(0001) has also been detected previously.[11, 19] The set of 18 islands contains representatives from three deposition temperatures. Examining the values as a function of T_{dep} (Fig. 7) shows no significant dependence of the structural quantities on temperature.

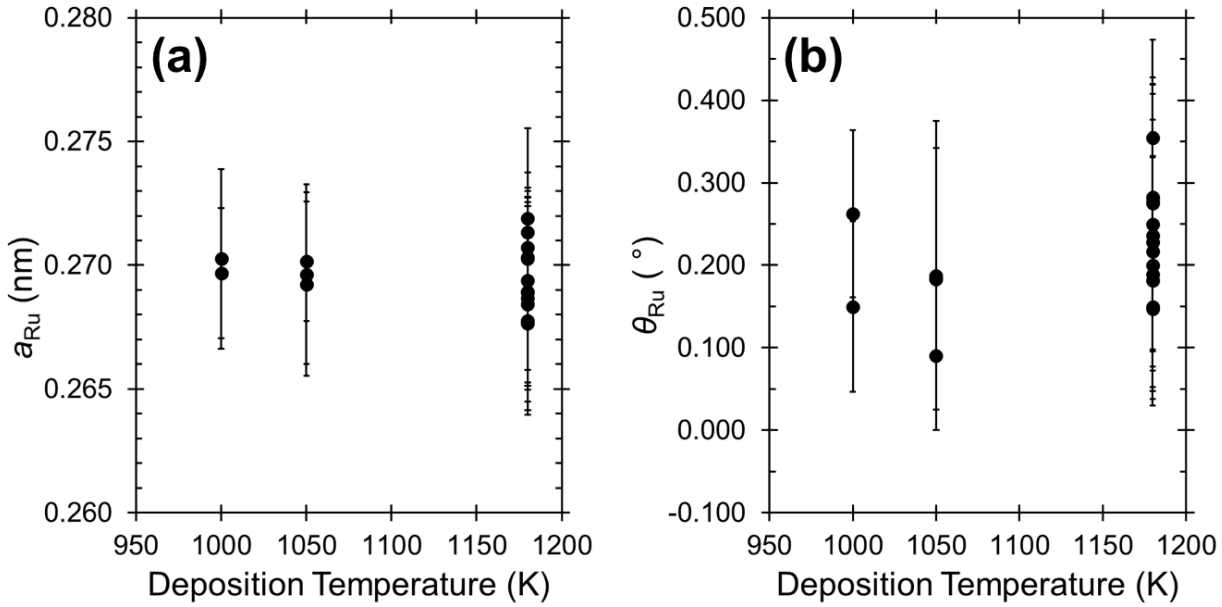

Figure 7. Values of (a) a_{Ru} and (b) θ_{Ru} as a function of deposition temperature, as determined from analyses of moiré patterns on Ru islands.

Evidence of single-layer graphene. Finally, close inspection reveals that the appearance of the carbon lattice depends on the position in the moiré. Figure 8a shows a zoomed-in image of the moiré and further shows the different appearance of the carbon lattice, enclosed by two boxes. In the yellow box that sits at a moiré minimum, the carbon lattice appears as triangular arrays where 3 out of 6 C atoms are visible. An enlarged image is shown in Fig. 8b. On the other hand, the blue box that is at a moiré maximum shows hollow honeycombs where all 6 C atoms are equally imaged (see Fig. 8c for enlargement). This difference arises from different interactions between monolayer graphene with the underlying Ru metal. At a moiré minimum, the C lattice is very close to the underlying Ru metal and thus interacts strongly with it. However, at the corrugated moiré maximum, the C lattice is lifted away from the Ru metal, causing the

interaction between C lattice and Ru to weaken. The C lattice thus becomes more "freestanding"[41] and all 6 C atoms are more equivalently imaged. This observation agrees with the appearance reported for the GML grown on bulk Ru(0001).[9-10] We have obtained atomic resolution on top of 19 embedded Ru islands, and all of them exhibit the honeycomb lattice at moiré maxima and triangular arrays at moiré minima, which is an expected behavior, both experimentally[10] and theoretically[41], of monolayer graphene on top of Ru(0001). The appearance of the C lattice is moiré-undulation dependent and thus is convincing evidence that these Ru islands are embedded under one graphene layer.

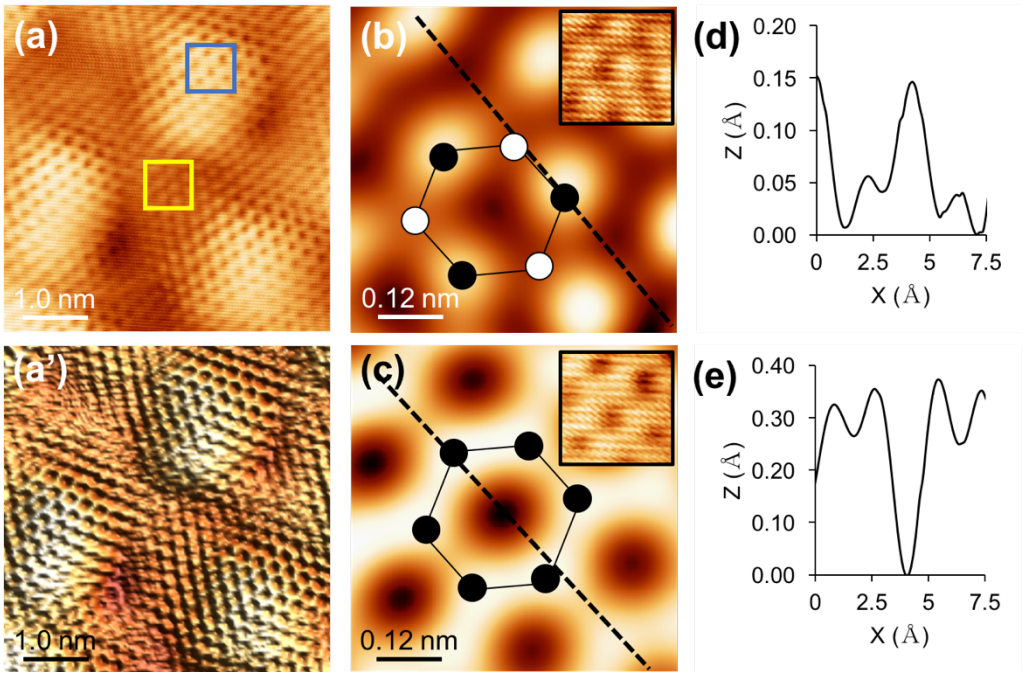

Figure 8. High-resolution images of moiré patterns on top of an embedded Ru island formed at 1050 K. (a) Moiré corrugations with different appearance of the C lattice depending on its location relative to the moiré. The lower (yellow) box sits at a moiré minimum, which shows triangular arrays of C lattice (3 out of 6 C atoms) with its enlargement further shown in (b). The top (blue) box sits at a moiré maximum where the C lattice is imaged as honeycombs (all 6 C atoms are equally imaged); (c) shows its enlargement. A semi-three-dimensional view is shown in (a'), where the hollow honeycombs are very visible around moiré maxima. (d,e) shows distinct profiles along diagonal dashed lines in (b,c) for different appearance of the C lattice. (a) is topographic. (b) and (c) are Fourier-filtered, while their insets show corresponding topographic images. Tunneling conditions are: (a,a',b,c) +3 mV, 0.41 nA.

Heights of embedded islands. In the simplest picture, island heights should cluster around discrete values separated by distances corresponding to interlayer spacings. However, analysis of 400 islands prepared at 1000 K < T_{dep} < 1180 K shows a noisy, nearly-continuous height distribution ranging from 0.4-1.3 nm. We attribute this to a combination of factors which complicate height determination: the uneven surface of the defect-rich graphitic substrate (visible in Fig. 5a-c), the moiré corrugation, deviations from mesa-like shapes, and irregularities sometimes present on the tops of Ru islands (e.g. Fig. 5c'). An additional contribution comes

from electronic effects in the height measurements, since the substrate (defect-rich graphite) differs from the island top (graphene on Ru). While this would normally contribute to uncertainty in absolute value of island height for fixed tunneling conditions, in our system there is an additional consideration: The electronic structure of the graphite substrate near an island must depend on the density and type of defects, since even a single isolated defect perturbs the electronic structure significantly over a range of several nm.[32, 36-37] This adds noise to the data.

The highest temperature, 1180 K, promotes the most regular islands. Thus from the islands at 1180 K, we select 51 islands with the most ideal profiles and obtain the height histogram shown in Fig. 9, with peaks at approximately 0.75 and 0.98 nm, and an estimated uncertainty of ± 0.03 nm. (Some individual profiles are shown in the SI.) The peak separation, 0.23 ± 0.04 nm, is consistent with the spacing between Ru(0001) planes, 0.214 nm.[16] Based upon DFT results to be presented in Sec. 3.5, the height of 0.75 nm is closest to that expected for 3-layer Ru islands. Thus, the histogram of measured heights indicates that both 3- and 4-layer islands are present at 1180 K. The smallest heights – in the range 0.4-0.6 nm – are populated at lower deposition temperature, and are closest to the value expected for 2-layer Ru islands.

To summarize, detailed examination of embedded Ru islands provides strong evidence that they are atomically well-ordered, are similar to bulk metal, have their close-packed planes parallel to the graphite surface, and are covered by a single graphene sheet. The range of island heights suggests that 2-4 atomic layers of Ru are present.

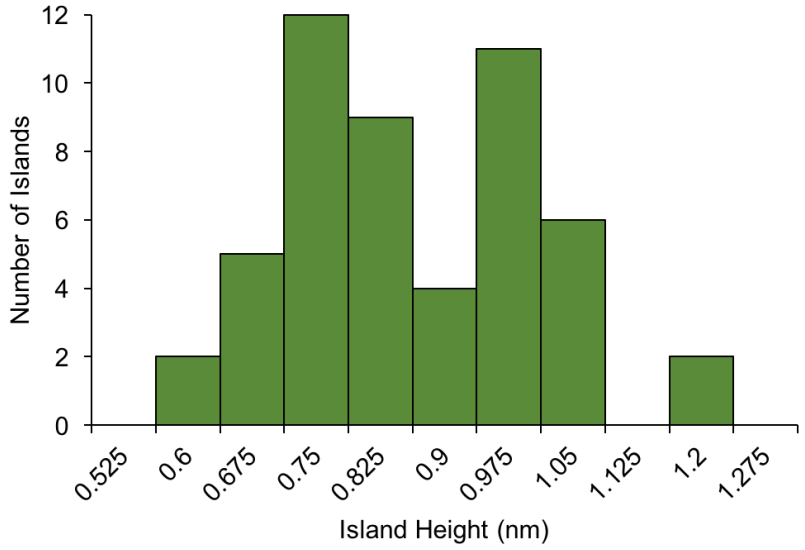

Figure 9. Height histogram of embedded Ru islands at 1180 K. The histogram includes 51 selected islands. Bin size is 0.075 nm.

3.4. Stability in air.

To test the stability of Ru islands in ambient conditions, we removed the sample from the UHV chamber and stored it in a desiccator for 5 months. The sample was then re-introduced to UHV, characterized, annealed at 800 K for 20 minutes, and characterized again. In Fig. 10a-c, the original XP spectrum of as-deposited Ru 3*d* is compared to that obtained after air exposure and UHV annealing. Remarkably, the peak positions of Ru ($3d_{5/2}$ and $3d_{3/2}$) do not shift, appearing at 280.0 and 284.1 eV for as-deposited, 279.9 and 284.1 eV for air-exposed, and 280.0 and 284.2 eV for vacuum outgassed samples. This is easily distinguishable from the B.E. of Ru $3d_{5/2}$ in Ru oxide, RuO_2, at 280.9 eV that is marked by a dashed line.[42] There are other forms of Ru oxides, RuO_3 and RuO_4, but their Ru $3d_{5/2}$ B.E. values are even higher, at 282.5 and 283.3 eV,[43] respectively.

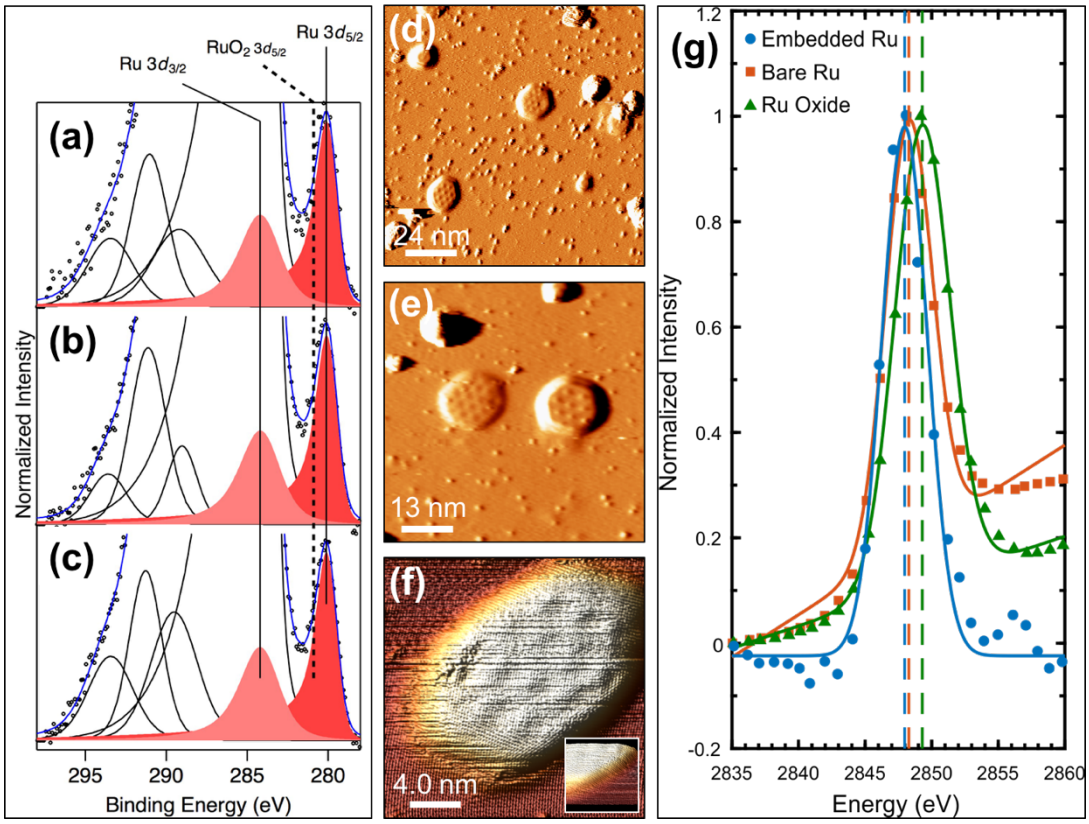

Figure 10. Characterization of samples with embedded Ru islands after air exposure. Left column: XPS of Ru 3*d* peaks after (a) Ru deposition at 1180 K, (b) air-exposure for 5 months, and (c) vacuum outgassing after air exposure. The vertical lines show the average binding energy of Ru $3d_{3/2}$ and Ru $3d_{5/2}$ peaks at 284.2 and 280.1 eV. Solid black curves show the C 1*s* main peak (truncated) and its loss features. Solid blue line shows the overall fit to the experimental data points. Intensities are normalized to the Ru $3d_{5/2}$ peak. Middle column: (d-e) Derivative STM images of Ru islands after 5 months of air exposure and annealing at 800 K for 20 minutes. (f) Example of an island that is atomically resolved after air exposure and annealing. Inset further shows the continuous graphene overlayer at the lower right edge of the island. Tunneling conditions are: (d,e) +1.4 V, 0.27 nA and (f) +0.4 V, 0.40 nA. (g) XAS of 2 graphite samples with deposited Ru, and commercial RuO_2 powder.

STM images were also acquired after air exposure and annealing in UHV, as shown in Fig. 10d-f. The graphite terraces appear more decorated after air exposure and outgassing. On top of some Ru islands, irregular and rough protruding features are observed, which are absent before air exposure. Nonetheless, most islands retain their faceted footprints and moiré patterns. The presence of the moiré is further support for absence of Ru oxidation. If oxygen had bonded and reacted with Ru, the graphene overlayer would have been decoupled from Ru, resulting in no moiré patterns.[44-45] The intact graphene overlayer, which survives air exposure (Fig. 10f), explains the long-term stability of the Ru islands in air.

Figure 10g shows XAS of the L_3 ($2p_{3/2}$) edge for samples with embedded Ru islands, bare Ru clusters, and RuO_2, transported in air but measured in high vacuum. Gaussian fits for each set of data show a shift in the peak positions (dashed lines) from embedded Ru at the lowest energy to RuO_2 at the highest energy. Values of peak positions and widths are given in the SI. The peak for embedded Ru is ~1.3 eV lower than that of RuO_2, whereas bare Ru is in between but much closer to embedded. Previous reports on Ru XAS have shown that the peak of Ru metal is at a lower energy than Sr_2RuO_4 [46] and that the XAS of Sr_2RuO_4 is very similar to that RuO_2 [47]. Our results for bare Ru clusters suggest that the XAS consists of a superposition of metallic signal and a minute amount of Ru oxide signal. In summary, the XAS data are consistent with the assertion that the embedded Ru islands are protected by the graphene sheet and retain their metallic character even after a long period (5 months) of exposure to air.

3.5. DFT results.

To assess the energetics of a metal cluster with n Ru atoms adsorbed on, or embedded beneath, the top GML, we define the chemical potential μ_{Ru} of the Ru atom as

$$\mu_{\mathrm{Ru}} = \frac{E_{\mathrm{tot}} - E_{\mathrm{graphite}}}{n} - E_{\mathrm{Ru}} \quad (1)$$

where E_{tot} is the total energy of the metal-plus-graphite system, E_{graphite} is the energy of graphite substrate, and E_{Ru} is the energy of one metal atom in gas phase. For one adatom (n = 1) adsorbed on the substrate, Eq. (1) reduces to the conventional expression for adsorption energy, $E_{\mathrm{ads}} = E_{\mathrm{tot}} - E_{\mathrm{graphite}} - E_{\mathrm{Ru}}$.

In the following calculations, we always use a 4-GML slab to mimic the graphite substrate, and a 2-nm vacuum thickness along the direction perpendicular to the slab surface. During relaxation for energy minimization, the bottom-most GML of the substrate is fixed. The energy cutoff is 600 eV. The force-convergence criterion is 0.1 eV/nm. All parameters are carefully tested for energy convergence.

For a single Ru atom, using 7×7×1 $\boldsymbol{k}$ mesh and a 6×6 supercell in units of a_{C}, we find that the minimum μ_{Ru} is -1.889 eV when the atom is adsorbed on top, and -2.903 eV when intercalated. Thus, intercalation of isolated Ru atoms is favored by 1.01 eV. Details of these calculations, as well as site-specific energetics, are given in the SI.

We also analyze systems with continuous hcp Ru(0001) films of 1-3 layers supported on graphite, and hcp Ru(0001) slabs of the same thickness embedded in graphite. Using an 11×11 supercell (in units of a_{C}) for the graphite substrate with a 10×10 supercell (in units of a_{Ru}) for Ru films results in Ru-graphite lateral lattice mismatch of $(11a_{\mathrm{C}} - 10a_{\mathrm{Ru}})/(10a_{\mathrm{Ru}})\times 100\% \approx -0.35\%$, i.e., a very small compressive strain in the Ru film parallel to the surface. We use this so-called 11-on-10 supercell in order to maintain the computations at a tractable size, as have

others,[48-50] even though a 12-on-11 supercell (with $11a_{\mathrm{Ru}}$ = 2.98 nm) would correspond more closely to the experimentally-observed unit cell length of 2.97 ± 0.13 nm for GML/Ru(0001) (Sec. 3.3). These calculations are very computationally-intensive, given the large unit cell with 242 C atoms per GML plus 100 Ru atoms per Ru monolayer (Ru ML), thick slabs, incorporation of van der Waals interactions, and significant relaxations that often affect all but the bottom-most GML. The most demanding calculations, e.g. for the 1268-atom system of 4 GMLs plus 3 Ru MLs, require on the order of 10^6 core-hours for convergence. The $\boldsymbol{k}$ mesh is $3\times3\times1$, while other calculation parameters are the same as those for the isolated atom. To determine the initial lattice position of the Ru film with respect to the substrate, we use a method similar to that in a previous study of GML/Ru(0001).[51]

Within this framework, μ_{Ru} is calculated using Eq. (1), where the metal cluster is taken as a Ru film of thickness L in units of Ru MLs. Table 1 shows μ_{Ru} at different values of L for Ru films adsorbed on, and slabs embedded in, graphite, as well as freestanding Ru films. Values of μ_{Ru} for a freestanding Ru film are always higher than the other cases, showing that a Ru film is stabilized by interaction with graphite. Also, with increasing L, μ_{Ru} approaches $-E_{\mathrm{coh}}$ of bulk hcp Ru (calculated as -7.150 eV), as it must. At any given L, μ_{Ru} is lower for the embedded slab than the adsorbed film, indicating that embedding a Ru slab for any L is energetically favored. With increasing L, the difference in μ_{Ru} between embedded and adsorbed film decreases, but is still significant even for L=3.

It is interesting to examine the structures of the fully-relaxed Ru film configurations (Fig. 11). For Ru *adsorbed on top* of graphite, the Ru ML at L=1 breaks up into clumps, while for larger L the adsorbed Ru layer remains contiguous. The underlying GML is weakly corrugated for L=1, but flat for larger L. By comparison, the *embedded* Ru ML is contiguous but with substantial rumpling at L=1. The corrugation of the embedded film decreases at L=2 and is almost gone at L=3. The embedded Ru film induces undulations, most prominently in the top GML but even in the two GMLs beneath, through L=3.

Some dimensions of the embedded Ru layers are determined from DFT (Table 1) and can be compared with experimental values. The island height, h, is quite low at L=1, which appears to be related to the deep rumpling of both Ru and graphene layers (Fig. 11b). The value of h=0.677 nm at L=3 is comparable to the experimentally-measured value of 0.75 nm (Fig. 9) though, as noted in Sec. 3.3, electronic effects and surface irregularities contribute uncertainty to the STM absolute value. Relative island heights should be less affected by this uncertainty. From DFT, Ru island heights are separated by distances Δh that exceed the spacing of 0.214 nm between (0001) planes in bulk Ru, i.e., Δh =0.278 nm between L=1,2 and Δh=0.259 nm between L=2,3. This is also apparently related to the Ru layer corrugation, so presumably, with increasing L and decreasing corrugation of the Ru layer, Δh converges to the bulk Ru spacing. From STM (Fig. 9), Δh=0.23±0.04 for L=3,4. This value is larger than that expected for bulk Ru, consistent with the DFT predictions.

The magnitude of corrugation of the top GML, c_{G}, is 0.157 nm at L=3 (Table 1). For comparison, values measured by STM in this work fall in the range 0.07-0.15 nm. For GML/Ru(0001), typical corrugations measured via STM are comparable: 0.08-0.15 nm.[9-10, 18-20] Values of 0.12-0.17 nm have been calculated with DFT for a single GML atop a 3-Ru ML slab.[41, 48, 51-55]

Table 1. μ_{Ru} (in eV/atom) vs. Ru(0001) film thickness L for freestanding, adsorbed, and embedded Ru films, from DFT. For the embedded films, some structural parameters are also derived from DFT. h is the average height of C atoms in the top GML, relative to the top surface of the graphite slab without Ru. Δh is the increase in h, relative to L-1. c_{G} is the corrugation of the top GML, defined as the height difference between highest and lowest C atoms in the top GML.

L	Freestanding Ru film	Adsorbed	Embedded	h (nm)	Δh (nm)	c_{G} (nm)
1	-4.398	-5.028	-5.202	0.140		0.234
2	-6.054	-6.143	-6.167	0.418	0.278	0.234
3	-6.418	-6.480	-6.502	0.677	0.259	0.157
bulk	-7.150				0.214	

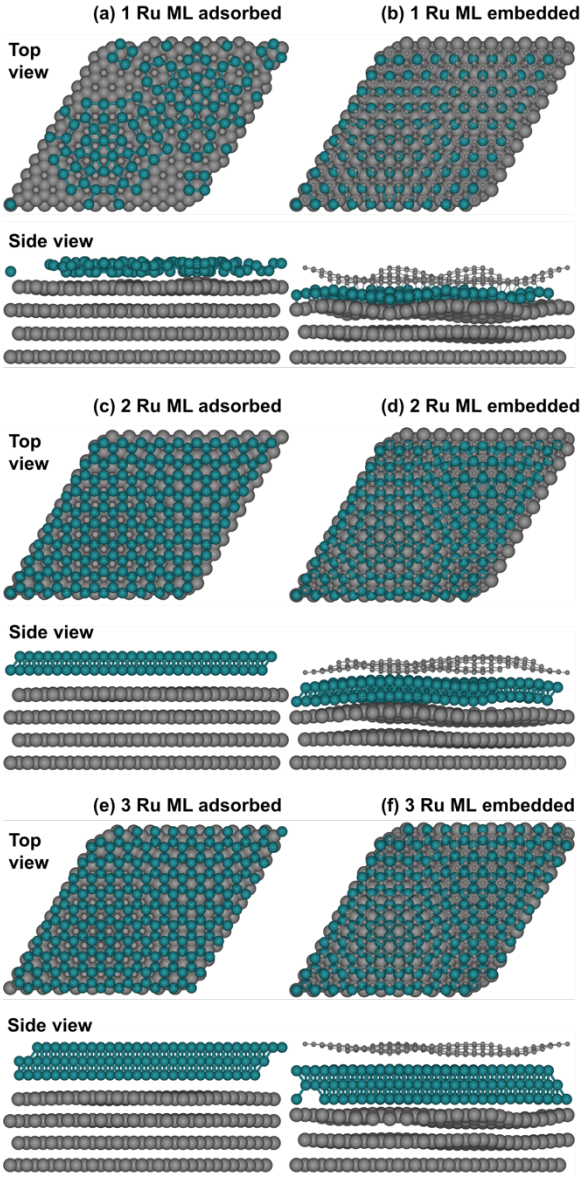

Figure 11. Fully-relaxed configurations of Ru(0001) films (blue), adsorbed on and embedded in, graphite (gray). These configurations correspond to those in Table 1.

4. Discussion.

Main results. The first broad conclusion from this work is that Ru forms metallic islands on graphite, covered by single-layer graphene. These islands are air-stable and contain 2-4 Ru MLs. However, they form only if the graphite surface is first ion-bombarded, then held at elevated temperature (1000-1180 K) during Ru deposition. A coincidence lattice forms between graphene and the Ru island top, which closely resembles that known for GML/Ru(0001), in terms of coincidence lattice constant, corrugation amplitude, and variation in carbon lattice appearance. Quantitative analysis of the graphene lattice in relation to the moiré is particularly revealing: It shows that the 2-dimensional lattice constant of the underlying metal equals that of bulk Ru(0001), within experimental error.

The second broad conclusion is that these embedded islands are energetically favored over on-top (adsorbed) islands, based on DFT for Ru films or slabs with L=1-3 layers. This can be understood in terms of strong Ru-C bonds forming at two interfaces rather than one. (Relatively strong bonding between graphene and Ru is well-established in the literature.[41, 44, 56-58]) Further, DFT shows that the relative stabilization of the embedded slab decreases with increasing L, which can be understood in terms of the decreasing relative contribution from the interfaces. This trend may explain why the embedded Ru islands exhibit only a limited range of thicknesses in experiment. It is not only slabs that are more stable in the carbon galleries; this is true also for individual Ru atoms. This is relevant to possible mechanisms of island formation, discussed below.

Mechanism of formation. We first consider the possibility that an embedded Ru island forms, by actually starting as an adsorbed (on-top) Ru island or cluster, through which C diffuses to ultimately form a graphene overlayer. We consider this because it is known that GMLs can be grown on the (0001) surface of bulk Ru by exploiting interstitial carbon dissolved in the bulk metal. The protocol involves heating the metal to temperatures of 1000-1400 K. During cooling, carbon segregates to the surface and forms graphene when the carbon concentration is high enough.[10, 13, 59-60] Furthermore, it is known that a C atom is easily extracted from the edge of graphene supported on Ru(0001), with a barrier of only 0.3 eV.[12] Thus, a Ru island could facilitate the creation of free C atoms, especially from defects in the underlying graphite.

There are several arguments against this mechanism of formation, however. First, adsorbed Ru clusters should be a precursor to the embedded islands, but the data do not show any obvious correlation between the two features. For instance, the density of embedded islands is roughly constant at 1000 K < T_{dep} < 1180 K, while density of bare clusters falls drastically (Fig. 3c). Second, embedded islands are not produced when a surface covered with bare Ru clusters is heated (Fig. 2a-l). Third, the graphene sheet is continuous from the graphite surface, up and over the embedded islands (Fig. 5, Fig. 6d). While we cannot exclude this mechanism, these observations make it unlikely.

Instead, we favor a model in which Ru atoms enter the carbon galleries through defects in the top graphene layer, then diffuse and nucleate in that space. Importantly, DFT shows that the first step in the process—movement of an adsorbed Ru atom into the gallery—is strongly favored energetically. Only a small fraction of defects has the appropriate size or configuration to act as entry portals. Elsewhere, we have shown that nucleation can take place at locations that are quite distant from the entry portal.[61]

A significant aspect of this model is that entry portals must remain open, rather than becoming clogged by Ru atoms, during Ru deposition. Calculations have shown that transition metal atoms bind very strongly to vacancies in graphene.[62] For atomic Ru, the calculated adsorption energy is -8.57 eV, -5.42 eV, and -2.09 eV at 1- and 2-atom vacancies and Stone-Wales defects, respectively.[63] A separate study yields a value of -8.15 eV at single-atom graphene vacancies.[64] This strong binding means that it is easy for metal islands to nucleate at portals and block them at low temperature. We propose that the high deposition temperature required in experiments serves the purpose of keeping portals open.

Comparison with other metals. It is of interest to compare the embedded Ru islands with those of Dy[5] and Cu[6]. The ranges of observed heights (in metal monolayers) is 2-4 for Ru, 3 for Dy, and roughly 10 to 200 for Cu. At the same time, the average island widths for Ru and Dy are comparable, falling in the range of about 10-20 nm, while Cu islands tend to be much broader, 30 to 570 nm. Thus, Ru bears most resemblance to Dy, and the comparison shows that a very wide range of encapsulated island dimensions are possible across different metals. At present, the factors contributing to this range are not understood, but modeling and experiments are underway to elucidate them. Another notable difference is in the deposition temperature necessary to form embedded islands. This is 600-800 K for Cu, 800-850 K for Dy, and 1000-1180 K for Ru. The much higher temperature for Ru suggests a correlation with cohesive energy, which is also much higher for Ru. The value for Ru is 6.74 eV/atom, versus 3.04 eV/atom for Dy and 3.49 eV/atom for Cu.[65] A relationship between deposition temperature and cohesive energy would be consistent with the conjecture above, namely, high deposition temperature serves the purpose of preventing metal cluster growth at portals.

5. Conclusions.

This detailed study shows that it is possible to grow nanoislands of multilayer Ru covered by a single layer of graphene, starting from a graphite surface. The nanoislands resemble bulk Ru(0001) in every measured respect. Embedded Ru islands are more stable than adsorbed Ru islands. Furthermore, we have shown that the embedded Ru islands are well-protected from extended atmospheric exposure. Our synthetic strategy opens up a new avenue to engineer Ru nanostructures near the surface of graphite or, conversely, to prepare nanodomains of Ru-supported graphene.

Acknowledgements

This work was supported mainly by the U.S. Department of Energy (DOE), Office of Science, Basic Energy Sciences, Materials Sciences and Engineering Division. Research was performed at the Ames Laboratory, which is operated by Iowa State University under contract No. DE-AC02-07CH11358. DFT calculations used resources of the National Energy Research Scientific Computing Center (NERSC), a U.S. DOE Office of Science User Facility operated under contract No. DE-AC02-05CH11231, and also used the Extreme Science and Engineering Discovery Environment (XSEDE), which is supported by National Science Foundation grant No. ACI-1548562. Use of the Advanced Photon Source, an Office of Science User Facility operated for the U.S. Department of Energy (DOE) Office of Science by Argonne National Laboratory, is

supported by the U.S. DOE under Contract No. DE-AC02-06CH11357. The experimental work was performed or supervised by ALR, DJ, NA, DV, MCT, and PAT. Theoretical work was performed or supervised by YH and JWE. KMY and MSA performed quantitative analyses on the lattice constants and orientations of embedded Ru islands. KMY and MSA gratefully acknowledge support from the Hong Kong Research Grants Council under grant 600113. JWE's participation in the theoretical work was supported by the DOE, Office of Science, Basic Energy Sciences, Chemical Sciences, Geosciences, and Biosciences Division. The data presented in this paper are available in DataShare (http://instr.iastate.libguides.com/datashare/home), an open data repository managed by Iowa State University.

References

1. Wintterlin, J.; Bocquet, M. L., Graphene on metal surfaces. *Surf. Sci.* **2009,** *603* (10), 1841-1852.
2. Batzill, M., The surface science of graphene: Metal interfaces, CVD synthesis, nanoribbons, chemical modifications, and defects. *Surf. Sci. Rep.* **2012,** *67* (3), 83-115.
3. Liu, X.; Han, Y.; Evans, J. W.; Engstfeld, A. K.; Behm, R. J.; Tringides, M. C.; Hupalo, M.; Lin, H.-Q.; Huang, L.; Ho, K.-M.; Appy, D.; Thiel, P. A.; Wang, C.-Z., Growth morphology and properties of metals on graphene. *Prog. Surf. Sci.* **2015,** *90* (4), 397-443.
4. Dresselhaus, M. S.; Dresselhaus, G., Intercalation compounds of graphite. *Adv. Phys.* **2002,** *51*, 1-186.
5. Zhou, Y.; Lii-Rosales, A.; Kim, M.; Wallingford, M.; Jing, D.; Tringides, M. C.; Wang, C.-Z.; Thiel, P. A., Defect-mediated, thermally-activated encapsulation of metals at the surface of graphite. *Carbon* **2018,** *127*, 305-311.
6. Lii-Rosales, A.; Han, Y.; Evans, J. W.; Jing, D.; Zhou, Y.; Tringides, M. C.; Kim, M.; Wang, C.-Z.; Thiel, P. A., Formation of Multilayer Cu Islands Embedded beneath the Surface of Graphite: Characterization and Fundamental Insights. *J. Phys. Chem. C* **2018,** *122* (8), 4454-4469.
7. Hagiwara, R.; Ito, M.; Ito, Y., Graphite intercalation compounds of lanthanide metals prepared in molten chlorides. *Carbon* **1996,** *34* (12), 1591-1593.
8. Büttner, M.; Choudhury, P.; Karl Johnson, J.; Yates, J. T., Vacancy clusters as entry ports for cesium intercalation in graphite. *Carbon* **2011,** *49* (12), 3937-3952.
9. Marchini, S.; Günther, S.; Wintterlin, J., Scanning tunneling microscopy of graphene on Ru(0001). *Phys. Rev. B* **2007,** *76* (7), 075429.
10. Sutter, E.; Acharya, D. P.; Sadowski, J. T.; Sutter, P., Scanning tunneling microscopy on epitaxial bilayer graphene on ruthenium (0001). *Appl. Phys. Lett.* **2009,** *94* (13), 133101.
11. Man, K. L.; Altman, M. S., Small-angle lattice rotations in graphene on Ru(0001). *Phys. Rev. B* **2011,** *84* (23), 235415.
12. Starodub, E.; Maier, S.; Stass, I.; Bartelt, N. C.; Feibelman, P. J.; Salmeron, M.; McCarty, K. F., Graphene growth by metal etching on Ru(0001). *Phys. Rev. B* **2009,** *80* (23), 235422.
13. Yi, P.; Haigang, Z.; Dongxia, S.; Jiatao, S.; Shixuan, D.; Feng, L.; Hong-jun, G., Highly Ordered, Millimeter-Scale, Continuous, Single-Crystalline Graphene Monolayer Formed on Ru (0001). *Adv. Mater.* **2009,** *21* (27), 2777-2780.
14. Sutter, E.; Albrecht, P.; Wang, B.; Bocquet, M.-L.; Wu, L.; Zhu, Y.; Sutter, P., Arrays of Ru nanoclusters with narrow size distribution templated by monolayer graphene on Ru. *Surf. Sci.* **2011,** *605* (17), 1676-1684.

15. Iannuzzi, M.; Kalichava, I.; Ma, H.; Leake, S. J.; Zhou, H.; Li, G.; Zhang, Y.; Bunk, O.; Gao, H.; Hutter, J.; Willmott, P. R.; Greber, T., Moiré beatings in graphene on Ru(0001). *Phys. Rev. B* **2013,** *88* (12), 125433.
16. Arblaster, J. W., Crystallographic Properties of Ruthenium. *Platin. Met. Rev.* **2013,** *57* (2), 127-136.
17. Martoccia, D.; Willmott, P. R.; Brugger, T.; Björck, M.; Günther, S.; Schlepütz, C. M.; Cervellino, A.; Pauli, S. A.; Patterson, B. D.; Marchini, S.; Wintterlin, J.; Moritz, W.; Greber, T., Graphene on Ru(0001): A 25 x 25 Supercell. *Phys. Rev. Lett.* **2008,** *101* (12), 126102.
18. Pan, Y.; Shi, D.-X.; Gao, H.-J., Formation of graphene on Ru(0001) surface. *Chin. Phys.* **2007,** *16* (11), 3151.
19. Bogdana, B.; Sara, B.; Manuela, G.; Marina, M.; Antonio, P.; Josefa, M. R.-G.; Juan Jose, H.; Daniel, F.; Amadeo, L. V. d. P.; Rodolfo, M., Electronic and geometric corrugation of periodically rippled, self-nanostructured graphene epitaxially grown on Ru(0001). *New J. Phys.* **2010,** *12* (9), 093018.
20. Gyamfi, M.; Eelbo, T.; Waśniowska, M.; Wiesendanger, R., Inhomogeneous electronic properties of monolayer graphene on Ru(0001). *Phys. Rev. B* **2011,** *83* (15), 153418.
21. Wang, B.; Bocquet, M. L.; Günther, S.; Wintterlin, J., Comment on "Periodically Rippled Graphene: Growth and Spatially Resolved Electronic Structure". *Phys. Rev. Lett.* **2008,** *101* (9), 099703.
22. de Parga, A. L. V.; Calleja, F.; Borca, B.; Passeggi, M. C. G.; Hinarejos, J. J.; Guinea, F.; Miranda, R., Vázquez de Parga et al. Reply. *Phys. Rev. Lett.* **2008,** *101* (9), 099704.
23. Schulz, H., Short history and present trends of Fischer–Tropsch synthesis. *Appl. Catal. A* **1999,** *186* (1), 3-12.
24. Serp, P.; Corrias, M.; Kalck, P., Carbon nanotubes and nanofibers in catalysis. *Appl. Catal. A* **2003,** *253* (2), 337-358.
25. Dong, L.; Gari, R. R. S.; Li, Z.; Craig, M. M.; Hou, S., Graphene-supported platinum and platinum–ruthenium nanoparticles with high electrocatalytic activity for methanol and ethanol oxidation. *Carbon* **2010,** *48* (3), 781-787.
26. Zhang, H.; Chu, W.; Zou, C.; Huang, Z.; Ye, Z.; Zhu, L., Promotion Effects of Platinum and Ruthenium on Carbon Nanotube Supported Cobalt Catalysts for Fischer–Tropsch Synthesis. *Catal. Lett.* **2011,** *141* (3), 438-444.
27. Li, G.; Kanezashi, M.; Tsuru, T., Catalytic Ammonia Decomposition over High-Performance Ru/Graphene Nanocomposites for Efficient COx-Free Hydrogen Production. *Catalysts* **2017,** *7* (1), 23.
28. G. Kresse, J. F., Efficient iterative schemes for ab initio total-energy calculations using a plane-wave basis set. *Phys. Rev. B* **1996,** *54*, 11169-11186.
29. Kresse, G.; Joubert, D., From ultrasoft pseudopotentials to the projector augmented-wave method. *Phys. Rev. B* **1999,** *59* (3), 1758-1775.
30. Jiří, K.; David, R. B.; Angelos, M., Chemical accuracy for the van der Waals density functional. *J. Phys.: Condens. Matter* **2010,** *22* (2), 022201.
31. Chung, D. D. L., Review graphite. *J. Mater. Sci.* **2002,** *37* (8), 1475-1489.
32. Hahn, J. R.; Kang, H., Vacancy and interstitial defects at graphite surfaces: Scanning tunneling microscopic study of the structure, electronic property, and yield for ion-induced defect creation. *Phys. Rev. B* **1999,** *60* (8), 6007-6017.
33. López, J. C. M.; Passeggi Jr, M. C. G.; Ferrón, J., Surface superstructures in highly oriented pyrolytic graphite surfaces after Ar^+ bombardment. *Surf. Sci.* **2008,** *602* (3), 671-676.

34. Habenicht, S.; Lieb, K. P.; Bolse, W.; Geyer, U.; Roccaforte, F.; Ronning, C., Ion beam erosion of graphite surfaces studied by STM: Ripples, self-affine roughening and near-surface damage accumulation. *Nucl. Instru. Meth. Phys. Res. B* **2000,** *161*, 958-962.
35. Habenicht, S.; Bolse, W.; Feldermann, H.; Geyer, U.; Hofsäss, H.; Lieb, K. P.; Roccaforte, F., Ripple topography of ion-beam–eroded graphite: A key to ion-beam–induced damage tracks. *Europhys. Lett.* **2000,** *50* (2), 209.
36. Mizes, H. A.; Foster, J. S., Long-range electronic perturbations caused by defects using scanning tunneling microscopy. *Science* **1989,** *244* (4904), 559-562.
37. Kushmerick, J. G.; Kelly, K. F.; Rust, H. P.; Halas, N. J.; Weiss, P. S., Observations of anisotropic electron scattering on graphite with a low-temperature scanning tunneling microscope. *J. Phys. Chem. B* **1999,** *103* (10), 1619-1622.
38. Nielsen, R. M.; Murphy, S.; Strebel, C.; Johansson, M.; Nielsen, J. H.; Chorkendorff, I., A comparative STM study of Ru nanoparticles deposited on HOPG by mass-selected gas aggregation versus thermal evaporation. *Surf. Sci.* **2009,** *603* (24), 3420-3430.
39. Morgan, D. J., Resolving ruthenium: XPS studies of common ruthenium materials. *Surf. Interface Anal.* **2015,** *47* (11), 1072-1079.
40. Hershberger, M. T.; Hupalo, M.; Thiel, P. A.; Tringides, M. C., Growth of fcc(111) Dy multi-height islands on 6H-SiC(0001) graphene. *J. Phys.-Condes. Matter* **2013,** *25* (22).
41. Wang, B.; Bocquet, M. L.; Marchini, S.; Gunther, S.; Wintterlin, J., Chemical origin of a graphene moire overlayer on Ru(0001). *Phys. Chem. Chem. Phys.* **2008,** *10* (24), 3530-3534.
42. Mc Evoy, A. J.; Gissler, W., ESCA Spectra and Electronic Properties of Some Ruthenium Compounds. *Phys. Status Solidi A* **1982,** *69* (1), K91-K96.
43. Kim, K. S.; Winograd, N., X-Ray photoelectron spectroscopic studies of ruthenium-oxygen surfaces. *J. Catal.* **1974,** *35* (1), 66-72.
44. Sutter, P.; Sadowski, J. T.; Sutter, E. A., Chemistry under Cover: Tuning Metal−Graphene Interaction by Reactive Intercalation. *J. Am. Chem. Soc.* **2010,** *132* (23), 8175-8179.
45. Lu, J.; Neto, A. H. C.; Loh, K. P., Transforming moiré blisters into geometric graphene nano-bubbles. *Nat. Commun.* **2012,** *3*, 823.
46. Chen, S.-A.; Liang, Y.-C.; Lu, K.-T.; Pao, C.-W.; Lee, J.-F.; Lin, T.-L.; Chen, J.-M., Atomic distribution and structural evolution of mesostructured PtRu nanoparticles electrodeposited on a microemulsion lyotropic liquid-crystalline template probed using EXAFS and XANES. *Phys. Chem. Chem. Phys.* **2014,** *16* (9), 3939-3945.
47. Hu, Z.; von Lips, H.; Golden, M. S.; Fink, J.; Kaindl, G.; de Groot, F. M. F.; Ebbinghaus, S.; Reller, A., Multiplet effects in the Ru L 2, 3 x-ray-absorption spectra of Ru(IV) and Ru(V) compounds. *Phys. Rev. B* **2000,** *61* (8), 5262-5266.
48. Wang, B.; Günther, S.; Wintterlin, J.; Bocquet, M. L., Periodicity, work function and reactivity of graphene on Ru(0001) from first principles. *New J. Phys.* **2010,** *12* (4), 043041.
49. Vázquez de Parga, A. L.; Calleja, F.; Borca, B.; Passeggi, M. C. G.; Hinarejos, J. J.; Guinea, F.; Miranda, R., Periodically Rippled Graphene: Growth and Spatially Resolved Electronic Structure. *Phys. Rev. Lett.* **2008,** *100* (5), 056807.
50. Stradi, D.; Barja, S.; Díaz, C.; Garnica, M.; Borca, B.; Hinarejos, J. J.; Sánchez-Portal, D.; Alcamí, M.; Arnau, A.; Vázquez de Parga, A. L.; Miranda, R.; Martín, F., Role of Dispersion Forces in the Structure of Graphene Monolayers on Ru Surfaces. *Phys. Rev. Lett.* **2011,** *106* (18), 186102.

51. Han, Y.; Evans, J. W., Adsorption and diffusion of Ru adatoms on Ru(0001)-supported graphene: Large-scale first-principles calculations. *J. Chem. Phys.* **2015,** *143* (16), 164706.
52. Jiang, D.-e.; Du, M.-H.; Dai, S., First principles study of the graphene/Ru(0001) interface. *J. Chem. Phys.* **2009,** *130* (7), 074705.
53. Semidey-Flecha, L.; Teng, D.; Habenicht, B. F.; Sholl, D. S.; Xu, Y., Adsorption and diffusion of the Rh and Au adatom on graphene moiré/Ru(0001). *J. Chem. Phys.* **2013,** *138* (18), 184710.
54. Zhang, L. Z.; Du, S. X.; Sun, J. T.; Huang, L.; Meng, L.; Xu, W. Y.; Pan, L. D.; Pan, Y.; Wang, Y. L.; Hofer, W. A.; Gao, H. J., Growth Mechanism of Metal Clusters on a Graphene/Ru(0001) Template. *Adv. Mater. Interfaces* **2014,** *1* (3), 1300104.
55. Iannuzzi, M.; Hutter, J., Comparative study of the nature of chemical bonding of corrugated graphene on Ru(0001) and Rh(111) by electronic structure calculations. *Surf. Sci.* **2011,** *605* (15), 1360-1368.
56. Preobrajenski, A. B.; Ng, M. L.; Vinogradov, A. S.; Mårtensson, N., Controlling graphene corrugation on lattice-mismatched substrates. *Phys. Rev. B* **2008,** *78* (7), 073401.
57. Brugger, T.; Günther, S.; Wang, B.; Dil, J. H.; Bocquet, M.-L.; Osterwalder, J.; Wintterlin, J.; Greber, T., Comparison of electronic structure and template function of single-layer graphene and a hexagonal boron nitride nanomesh on Ru(0001). *Phys. Rev. B* **2009,** *79* (4), 045407.
58. Sutter, P.; Hybertsen, M. S.; Sadowski, J. T.; Sutter, E., Electronic Structure of Few-Layer Epitaxial Graphene on Ru(0001). *Nano Lett.* **2009,** *9* (7), 2654-2660.
59. Sutter, P. W.; Flege, J.-I.; Sutter, E. A., Epitaxial graphene on ruthenium. *Nat. Mater.* **2008,** *7*, 406.
60. McCarty, K. F.; Feibelman, P. J.; Loginova, E.; Bartelt, N. C., Kinetics and thermodynamics of carbon segregation and graphene growth on Ru(0001). *Carbon* **2009,** *47* (7), 1806-1813.
61. Han, Y.; Lii-Rosales, A.; Zhou, Y.; Wang, C. J.; Kim, M.; Tringides, M. C.; Wang, C. Z.; Thiel, P. A.; Evans, J. W., Nucleation and growth kinetics for intercalated islands during deposition on layered materials with isolated pointlike surface defects. *Phys. Rev. Mater.* **2017,** *1* (5), 053403.
62. Krasheninnikov, A. V.; Lehtinen, P. O.; Foster, A. S.; Pyykkö, P.; Nieminen, R. M., Embedding Transition-Metal Atoms in Graphene: Structure, Bonding, and Magnetism. *Phys. Rev. Lett.* **2009,** *102* (12), 126807.
63. Guo, X.; Liu, S.; Huang, S., Single Ru atom supported on defective graphene for water splitting: DFT and microkinetic investigation. *Int. J. Hydrog. Energy* **2018,** *43* (10), 4880-4892.
64. N., S. D.; Željko, Š.; N., B. E.; R., B. M., Formic Acid Synthesis by CO_2 Hydrogenation over Single-Atom Catalysts Based on Ru and Cu Embedded in Graphene. *ChemistrySelect* **2018,** *3* (9), 2631-2637.
65. Kittel, C., *Introduction to Solid State Physics*. 7 ed.; John Wiley & Sons: New York, 1996.